A&A 536, A91 (2011)
DOI: 10.1051/0004-6361/201014821

Astronomy & Astrophysics

Sulfur depletion in dense clouds and circumstellar regions

I. H_2S ice abundance and UV-photochemical reactions in the H_2O-matrix

A. Jiménez-Escobar and G. M. Muñoz Caro

Centro de Astrobiología, Dpto. de Astrofísica, INTA-CSIC, Carretera de Ajalvir, km 4, Torrejón de Ardoz, 28850 Madrid, Spain
e-mail: jimenezea@cab.inta-csic.es

Received 19 April 2010 / Accepted 13 October 2011

ABSTRACT

Aims. This work aims to study the unexplained sulfur depletion observed toward dense clouds and protostars.
Methods. We made simulation experiments of the UV-photoprocessing and sublimation of H_2S and H_2S:H_2O ice in dense clouds and circumstellar regions, using the InterStellar Astrochemistry Chamber (ISAC), a state-of-the-art ultra-high-vacuum setup. The ice was monitored in situ by mid-infrared spectroscopy in transmittance. Temperature-programmed desorption (TPD) of the ice was performed using a quadrupole mass spectrometer (QMS) to detect the volatiles desorbing from the ice.
Results. Comparing our laboratory data to infrared observations of protostars we obtained a more accurate upper limit of the abundance of H_2S ice toward these objects. We determined the desorption temperature of H_2S ice, which depends on the initial H_2S:H_2O ratio. UV-photoprocessing of H_2S:H_2O ice led to the formation of several species. Among them, H_2S_2 was found to photodissociate forming S_2 and, by elongation, other species up to S_8, which are refractory at room temperature. A large fraction of the missing sulfur in dense clouds and circumstellar regions could thus be polymeric sulfur residing in dust grains.

Key words. ISM: molecules – methods: laboratory – ultraviolet: ISM – dust, extinction – infrared: ISM

1. Introduction

Sulfur is depleted in molecular clouds by a factor of 1000 compared to its estimated cosmic abundance (Tieftrunk et al. 1994), while in the diffuse interstellar medium the abundance of sulfur in the gas phase is comparable to the cosmic abundance. This suggests that there is a form of sulfur in the gas phase that was not observed in molecular clouds, which could be atomic sulfur, or alternatively that sulfur chemistry on icy grain mantles, present in dense clouds and regions around young stellar objects (YSOs) but not in the diffuse interstellar medium, plays an important role.

There is compelling evidence that supports the role of dust grains on sulfur chemistry. Several gas-phase S-containing molecules were observed in hot cores, such as OCS, H_2S, H_2CS, SO, SO_2, HCS^+, and NS (van der Tak et al. 2003). Current gas-phase chemical models are unable to explain the abundances of S-species like HCS^+ and OCS measured toward protostars (Doty et al. 2004). The depletion of sulfur is observed not only in dense clouds, but also toward Class 0 and Class I sources (Buckle & Fuller 2003) and toward hot cores (Wakelam et al. 2004). The abundances of S-bearing species, including H_2S, suggest that these molecules are formed on grain surfaces and subsequently released to the gas phase.

Several S-bearing molecules have been detected in comets. Among them H_2S has the largest abundance, from 0.2 to 1.5% relative to H_2O (Irvine et al. 2000). There seems to be a general agreement between the molecular abundances observed in circumstellar ices and in comets (Bockelée-Morvan et al. 2000). That suggests that H_2S is expected to be present in circumstellar ice mantles. The H_2S ice will be strongly processed by UV and ion irradiation (Garozzo et al. 2010; Grim & Greenberg 1987; Moore et al. 2007).

We explore here the possibility that the missing sulfur atoms may be present in icy grain mantles. The cosmic abundance of sulfur is 1.23×10^{-5} N_H, or 37 times less abundant than oxygen (Snow & Witt 1996), and like oxygen, sulfur belongs to group 16 of the periodic table. The electronegativity values of S and O are 2.58 and 3.44 on the Pauling scale, and the electron affinities are 200 and 141 kJ mol^{-1}. The bond energy of an S−H bond is 363 kJ mol^{-1}, while that of an O−H bond is 458.9 kJ mol^{-1}, and therefore S−H bond formation is favored over O−H bond formation. Given that H is the most abundant element, S atoms will tend to form H_2S molecules because they impinge on icy grain mantles. The feature due to the stretching mode of H_2S at 3.925 μm (2548 cm^{-1}) has a band strength of $A \approx 2.9 \times 10^{-17}$ cm molecule^{-1} (Smith 1991), and $A(H_2O) = 2.0 \times 10^{-16}$ cm molecule^{-1} (Hagen et al. 1981). Therefore, if we make the crude assumption that the H_2S abundance in the ice is roughly about 1/37 that of H_2O ice, based on the S/O = 1/37 cosmic abundance ratio, the absorbance area of H_2S relative to that of H_2O might just be 0.4%, which is close to the detection limit of most observations. With the exception of a weak CH_3OH absorption, the feature falls on a relatively *clean* part of the mid-infrared spectrum. If present, it might be observable in the spectra of circumstellar or dense interstellar icy grains.

Solid H_2S has not been detected in the interstellar medium. The presence of H_2S ice was inferred in W33A, a high-mass protostar (Geballe et al. 1985; Geballe 1991), and a band at 4.9 μm (2040 cm^{-1}) was attributed to OCS (Geballe et al. 1985; Palumbo et al. 1995). The detection of OCS is possible since the 4.9 μm band has a considerable band strength, $A = 1.5 \times 10^{-16}$ cm molecule^{-1} (Hudgins et al. 1993). In addition

to OCS, SO_2 was detected in ice mantles (Boogert et al. 1997). The H_2S detection by Geballe is not fully supported in the literature. Van der Tak et al. (2003) argue that infrared observations do not support the assumption that H_2S is the main S reservoir in grain mantles, and they provide the ISO-SWS observations of W33A as an example. One of the problems for identifying the 3.925 μm (2548 cm^{-1}) band of H_2S in H_2O-rich ice mantles was the lack of laboratory spectra of H_2S embedded in an H_2O matrix, which is expected to affect this band significantly.

Ultraviolet emission spectra of the coma of comet IRAS-Araki-Alcock showed the presence of S_2, and the spatial profiles indicate a release of this species directly from, or very close to, the nucleus (A'Hearn et al. 1983). Diatomic sulfur was later found in the comet Hyakutake (Laffont et al. 1996). Based on the formation of S_2 at 12 K from irradiation of dirty ice containing H_2S, Grim & Greenberg (1987) suggested that S_2 was formed in interstellar ice mantles that ultimately aggregate into comets. Subsequently, fast reactions between OCS and metastable S, produced during the dissociation of CS_2, were proposed. This supports the formation of S_2 in the coma (e.g., A'Hearn et al. 2000). The formation of polymeric sulfur in interstellar environments involves the dissociation of H_2S and might, therefore, serve as a probe of energetic processing of the precometary ice. Ion irradiation experiments of ice analogs containing CO, CH_3OH, and S-bearing species lead to formation of OCS and CS_2 molecules (Ferrante et al. 2008; Garozzo et al. 2010).

Previously, we performed an experiment consisting of the photoprocessing of H_2O:CO:NH_3:H_2S ice followed by warm-up to room temperature. This residue was analyzed by means of gas chromatography coupled to mass spectroscopy. Among the residue products several N-heterocycles and a number of S-bearing molecules were detected. S-polymers, S_6 through S_8, were formed, resulting from the S atoms released after photodissociation of H_2S ice. But also pentathian (S_5CH_2), hexathiepan (S_6CH_2), and c-(S-CH_2-NH-CH_2-NH-CH_2) were detected (Muñoz Caro 2002). The presence of S-containing refractory molecules in icy grain mantles, like sulfur polymers, might be the reservoir of the missing sulfur in dense clouds and circumstellar environments (Wakelam et al. 2005).

To approach the S-depletion dilemma in dense clouds and YSOs, we carried out a series of experiments on the deposition of pure H_2S or H_2S in an H_2O-matrix under UHV conditions at 7 K, to mimic interstellar/circumstellar conditions followed by warm-up. We measured the mid-infrared spectra of both pure H_2S ice and H_2S in an H_2O ice matrix at different temperatures from 7 K to sublimation. Similar spectra were reported by Moore et al. (2007) at higher temperatures. Using a quadrupole mass spectrometer (QMS), we obtained the temperature programmed desorption (TPD) plots showing the abundances of the molecules released to the gas phase as a function of temperature during warm-up. These experiments were repeated, including UV irradiation of the ice. The infrared spectra of H_2S ice measured in the laboratory were compared with spectroscopic observations performed by ISO, providing new upper limits on the H_2S abundance toward protostars.

The layout of this paper is as follows. In Sect. 2 we describe the experimental protocol. The experimental results are presented in Sect. 3. The astrophysical implications are discussed in Sect. 4, and the main conclusions summarized in Sect. 5.

2. Experimental

The experiments were performed using the InterStellar Astrochemistry Chamber (ISAC). This set-up and the standard experimental protocol were described in Muñoz Caro et al. (2010). ISAC mainly consists of an ultra high vacuum (UHV) chamber, with pressure typically in the range $P = 2.5–4.0 \times 10^{-11}$ mbar, where an ice layer made by deposition of a gas mixture onto a cold finger at 7 K, achieved by means of a closed-cycle helium cryostat, can be UV irradiated.

Samples can be heated in a controlled way from 7 K to room temperature, allowing TPD experiments of ices. The evolution of the solid sample was monitored by in situ transmittance FTIR spectroscopy, while the volatile species were detected by QMS. The gas line works dynamically, and allows the deposition of gas mixtures with the desired composition, which is monitored in real time by QMS. A second deposition tube was used for co-deposition of corrosive gases, such as NH_3 or H_2S. A prechamber is used to extract the samples while preserving the UHV in the main chamber.

The chemical components used for the experiments described in this paper were H_2O (liquid), triply distilled, and H_2S (gas), Praxair 99.8%. H_2S was deposited through the second deposition tube to prevent it from reacting with H_2O vapor prior to deposition. For the irradiation experiments, the deposited ice layer was photoprocessed with a microwave-stimulated hydrogen flow discharge lamp. The lamp output is $\approx 1.5 \times 10^{15}$ photons s^{-1} (Weber & Greenberg 1985), and the flux was measured at the sample position using oxygen actinometry is $I_0 = 2.5 \times 10^{14}$ photons cm^{-2} s^{-1}, see Muñoz Caro et al. (2010) for details. The emission spectrum of the lamp ranges from 7.3 to 10.5 eV (with an average photon energy of 9.2 eV), with main emission at Lyman-α (10.2 eV) for a hydrogen pressure $P_H = 0.5$ torr.

Except for experiment S2 and S6, with resolution 1 cm^{-1}, the spectral resolution was generally 4 cm^{-1} to allow acquisition of spectra during continuous warm-up. The column density of the deposited ice was calculated using the formula

$$N = \int_{\text{band}} \frac{\tau_\nu \mathrm{d}\nu}{A} \quad (1)$$

where N is the column density in cm^{-2}, τ the optical depth of the band, dν the wavenumber differential in cm^{-1}, and A the band strength in cm molecule^{-1}. The adopted band strength for H_2O at 3.05 μm (3279 cm^{-1}) was given in Sect. 1, $A(H_2O) = 2.0 \times 10^{-16}$ cm molecule^{-1} (Hagen et al. 1981). For H_2S, we used $A(H_2S) = 2.9 \times 10^{-17}$ cm molecule^{-1} (Smith 1991) at 70–80 K. Around 10 K we estimated $A(H_2S) = 2.0 \times 10^{-17}$ cm molecule^{-1}, see Sect. 3.1. The column density per number of S atoms in molecule X, $N_s(X)$, corresponds to $N_s(X) = N(X)n_S(X)$, where $n_S(X)$ is the number of S atoms in molecule X.

Experiments S7 to S11 involved deposition of the ice layer followed by UV irradiation. The ice mixture compositions were obtained by integrating the infrared absorption bands after deposition. The values in Table 1 correspond to the column density of H_2S mixed with H_2O ice. They were calculated assuming that the band strength value is equal to that in pure H_2S ice. Except for experiment S12, the experiments reported here involved irradiation times shorter than two hours. Calibration experiments of the UV flux using actinometry (Muñoz Caro et al. 2010), performed before and after the experiments, showed that the flux remains constant during two hours irradiation. For longer irradiation times of five-hour, we found that the flux decreases by 11%. Therefore, the UV photon fluence, in photon cm^{-2}, is the product of the UV flux value given above, I_0, by the irradiation time, t in seconds:

$$Fluence = I_0 t. \quad (2)$$

Table 1. Parameters of the experiments.

Exp. S#	Comment	Ice mixture H_2S:H_2O	Fluence $\frac{\text{photons}}{\text{cm}^2}$	Heating rate $\frac{\text{K}}{\text{min}}$	$N(H_2S)$ cm^{-2}	$\frac{N_S(HS_2^{\cdot})}{N_S(H_2S)}$ (%)	$1-\frac{N_S(H_2S)}{N_S(H_2S)_i}$ (%)
1	Deposition	1:0	–	1.1	1.2×10^{16}	–	–
2	Deposition	1:0	–	0.5	6.8×10^{16}	–	–
3	Deposition	1:0	–	1.3	8.4×10^{16}	–	–
4	Deposition	1:0	–	1.0	6.8×10^{16}	–	–
5	Deposition	13.7:100	–	2.0	1.5×10^{16a}	–	–
6	Deposition	7.5:100	–	1.0	1.3×10^{16a}	–	–
7	Dep., after irrad.	1:0	1.6×10^{18}	3.3	7.0×10^{16}	36.(±9)	90(±1)
8	Dep., after irrad.	1:0	1.5×10^{18}	1.4	9.9×10^{16}	34.(±8)	82(±1)
9	Dep., after irrad.	1:0	1.5×10^{18}	2.1	3.7×10^{16}	25.(±6)	96(±1)
10	Dep., after irrad.	4.0:100	6.0×10^{17}	1.0	3.0×10^{16a}	–	75(±1)
11	Dep., after irrad.	8.8:100	6.0×10^{17}	1.0	1.6×10^{16a}	–	78(±1)
12	Simultaneus dep. and irrad.	13:100	3.8×10^{18}	1.0	3.8×10^{17}	–	–

Notes. [(a)] Column density of H_2S obtained from integration of infrared absorption assuming $A(H_2S)_{\text{pure}} = A(H_2S)_{\text{mixed}} = 2.0 \times 10^{-17}$ cm molec^{-1}.

Mason et al. (2006) measure the VUV spectra in the [6.0−10.5 eV] range for different molecules in the gas and solid phases. The Ly-α cross section value of water at 25 K obtained from Mason data is 4.0×10^{-18} cm^2. The UV absorbed by the ice in our experiments was monitored using

$$UV\text{absorption} = \frac{I_0 - I}{I_0} = 1 - \frac{I}{I_0} = 1 - \exp\left(-\sigma N(\text{ice})\right) \quad (3)$$

where I_0 is the above value for the incident UV photon flux at the sample position, I the outgoing UV photon flux, σ the UV absorption cross section of the ice, and N(ice) the total ice column density. The thickest irradiation, experiment S10, was performed with a total ice thickness of 0.25 μm where 95% of the impinging photons are absorbed by the ice according to Eq. (3). For H_2S ice, there is no reported σ value. We adopt the value of 9.01×10^{-16} cm^{2}nm in the [121.2−159.3 nm] range or 6.7×10^{-18} cm^2 per photon of 9.2 eV for H_2S in the gas phase (Lee et al. 1987). For experiment S8, corresponding to the thickest layer of pure H_2S, we find that the UV transmission of H_2S ice drops to 51% for 0.032 μm.

Experiment S12 differs from the others because it involved simultaneous deposition and irradiation. The gas was condensed at a rate of about 2.5×10^{14} molecules cm^{-2} s^{-1}. Because the UV flux is 2.5×10^{14} photons cm^{-2} s^{-1}, very roughly, the ice was exposed to about one photon per molecule on average. For this experiment the column density of the ice was estimated as follows. The H_2O:H_2S = 13:100 ratio of the gas mixture in the gas line during deposition was measured by QMS and found to remain constant. The deposition rate, in molecules cm^{-2}s^{-1}, was calibrated from previous experiments, allowing the estimation of the total ice column density for a total deposition time of 252 min. and in particular the value of $N(H_2S)$ given in Table 1.

3. Experimental results

Table 1 lists the experimental parameters. The first three columns indicate, respectively, the label of the experiment, if the experiment involved irradiation, and the starting ice composition. The fourth column gives the fluence in photons cm^{-2}, the fifth column the heating rate in K min^{-1}. The sixth column is the column density of deposited H_2S ice. In experiment S12 the column density of H_2S was inferred from gas phase composition during deposition and irradiation (QMS data) and calibration with previous experiments. The deposition rate (in molecules cm^{-2} s^{-1}) of the ice in that experiment was chosen to be equal to the lamp flux (photons cm^{-2} s^{-1}). The seventh column is the column density of $HS_2^{\cdot}$ after 100 min irradiation, $N_s(HS_2^{\cdot}) = 2\,N(HS_2^{\cdot})$, divided by the column density of deposited H_2S, $N_s(H_2S) = N(H_2S)$, in percent, obtained from integration of the infrared bands. These are the three experimental points in Fig. 7 (bottom panel) for around 100 min of irradiation. No value of $A(HS_2^{\cdot})$, the band strength of $HS_2^{\cdot}$, was found in the literature. We assumed $A(HS_2^{\cdot}) = 0.5\,A(H_2S)$ because H_2S has 2 S−H bonds while $HS_2^{\cdot}$ only has one. The values obtained are affected by an error of 25 %. The last column provides an upper limit value for the total of products in percent, estimated from the decrease in the infrared H_2S band at 3.925 μm (2548 cm^{-1}) upon irradiation, i.e. $1-\frac{N_s(H_2S)}{N_s(H_2S)_i}$ where $N_s(H_2S)_i$ is the initial column density of H_2S in the ice and $N_s(H_2S)$ the column density after irradiation, assuming that all the photolyzed H_2S molecules led to product formation.

Section 3.1 describes the results from the experiments consisting on the deposition and controlled warm-up of pure H_2S ice, experiments S1 to S4, or H_2S in an H_2O-matrix, experiments S5 and S6. Section 3.2 describes the results from experiments S7 to S9, where the ice was irradiated after deposition. Section 3.3 describes experiments S10 and S11 involving the deposition of H_2S:H_2O ice mixtures followed by irradiation, and experiment S12, involving simultaneous deposition and irradiation.

3.1. Annealing of H_2S ice experiments

The top panel of Fig. 1 displays the infrared band of pure H_2S at 1 cm^{-1} spectral resolution after deposition at 7 K and during warm-up to 90 K, the temperature at which sublimation was complete. The band of H_2S ice at 7 K, considered to be amorphous, reaches its maximum around 2543 cm^{-1} (3.93 μm). Crystallization is expected to take place during warm-up and as a result, the different vibrational modes become better defined. This is shown as a change in the band profile, which is observed around 40 K, leading to three subfeatures that were attributed to 2551 cm^{-1} (ν_3, antisym. HS-str.), 2528 cm^{-1} (ν_1, sym. HS-str.), and 2539 cm^{-1}, which could be due to the remaining amorphous H_2S. We performed a similar experiment depositing a thick H_2S ice layer to detect the weak H-S bending mode. The bottom panel of Fig. 1 shows the stretching mode of crystalline H_2S and the inlet shows the bending mode around 1169 cm^{-1} (8.554 μm).

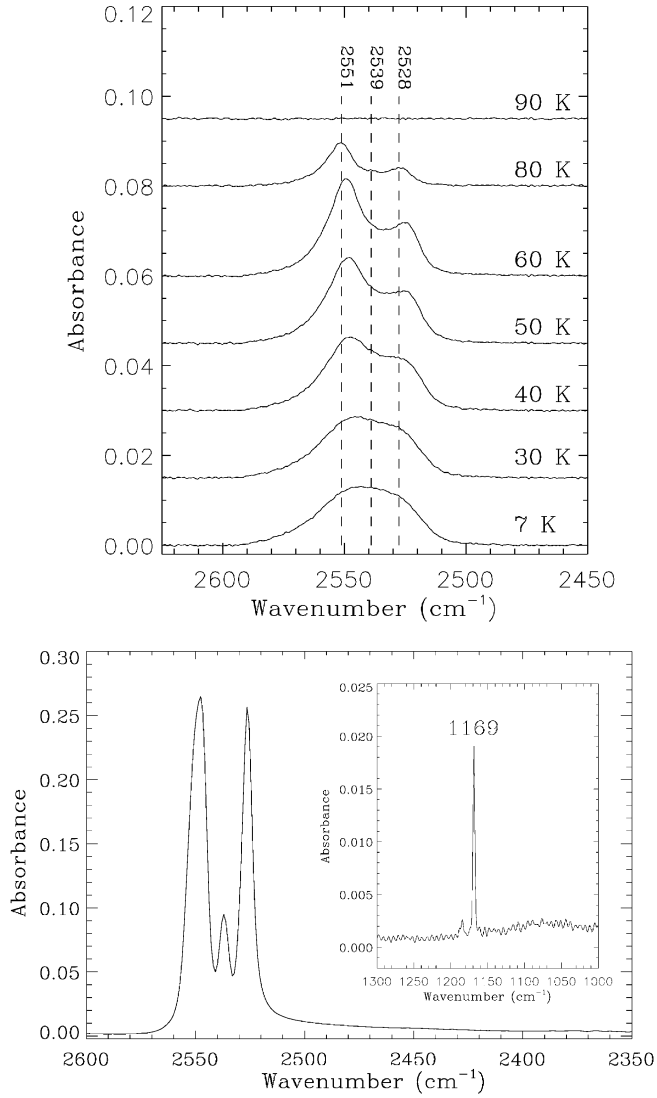

Fig. 1. *Top*: infrared spectra of H_2S ice with 1 cm^{-1} spectral resolution at different temperatures during warm-up, corresponding to experiment S2 of Table 1. *Bottom*: infrared spectrum showing the stretching modes of crystalline H_2S deposited at 70 K. Inlet shows the bending mode absorption.

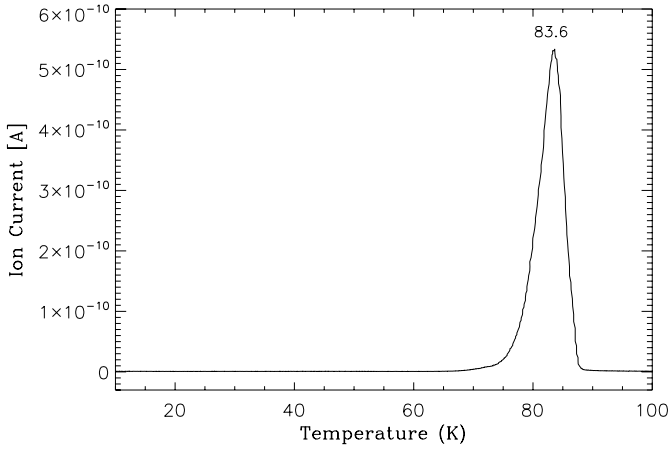

Fig. 2. Thermal desorption of pure H_2S, with a heating rate of 1.0 K min^{-1}, corresponding to experiment S4 of Table 1. The ion current in Ampere, represented on the y-scale, corresponds roughly to the partial pressure in mbar.

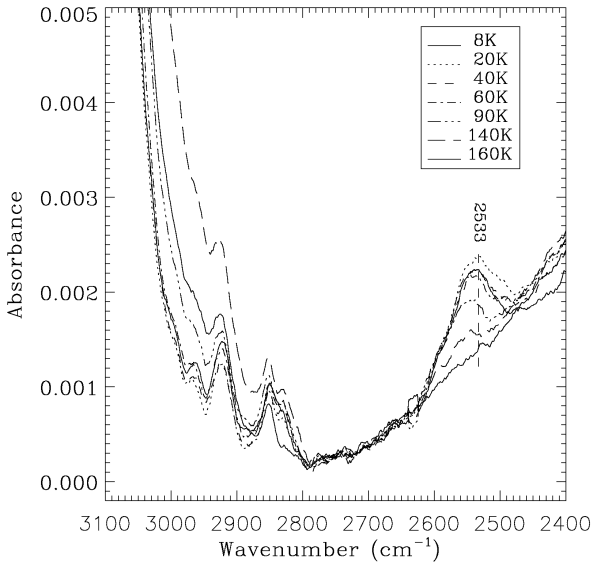

Fig. 3. Infrared spectra of the H_2S:H_2O = 7.5:100 ice mixture at different temperatures during warm-up, corresponding to experiment S6 of Table 1.

Our spectra are similar to those previously published, see Moore et al. (2007) and ref. therein.

During sequential warm-up, H_2S ice sublimation is also traced by the detection of gas phase molecules at the QMS located on the main chamber of ISAC. This QMS data, henceforth referred to as the TPD curve, is displayed in Fig. 2 for m/z = 34. Around 70 K a very sharp increase in the TPD curve is observed, see Fig. 2. That corresponds to the sublimation stage of the ice.

To study the effect of the H_2O-matrix, we deposited an H_2S:H_2O = 7.5:100 ice mixture, see experiment S6 parameters in Table 1. Figure 3 shows the infrared band of H_2S for this experiment at 1 cm^{-1} spectral resolution. The main effect of the interaction between H_2O and H_2S molecules in the solid is the widening of the H_2S band (FWHM of 75 cm^{-1} for H_2S in an H_2O ice matrix compared to 43 cm^{-1} for pure H_2S ice), see Fig. 3. The wavenumber position of the H_2S infrared band does not change significantly when mixed with H_2O. The TPD data collected during this experiment are shown in Fig. 4. The TPD curve of H_2O for m/z = 18 in Fig. 4 is similar to the one of pure H_2O ice, which is not shown. The data show the transitions from amorphous solid water (asw) of low density to cubic ice (Ic) at 130−140 K, and from cubic ice (Ic) to hexagonal ice (Ih) around 150 K (Hagen et al. 1981). On the other hand, the H_2O matrix has a strong effect on the desorption of H_2S ice, as inferred from comparison of the TPD curve of pure H_2S, see Fig. 2 for m/z = 34, with the TPD curve of H_2S in experiment S6, see Fig. 4 for m/z = 34. The maximum around 82 K in Fig. 4 corresponds to the observed peak for pure H_2S in Fig. 2. The peaks around 145 and 163 K were not observed for pure H_2S ice, which indicates that a fraction of the H_2S molecules are retained at higher temperatures in the H_2O-matrix. The desorption peak of H_2S around 145 K forms during the sublimation of the H_2O ice bulk, while the less intense peak around 163 K appears right after the maximum in the sublimation of H_2O around 160 K.

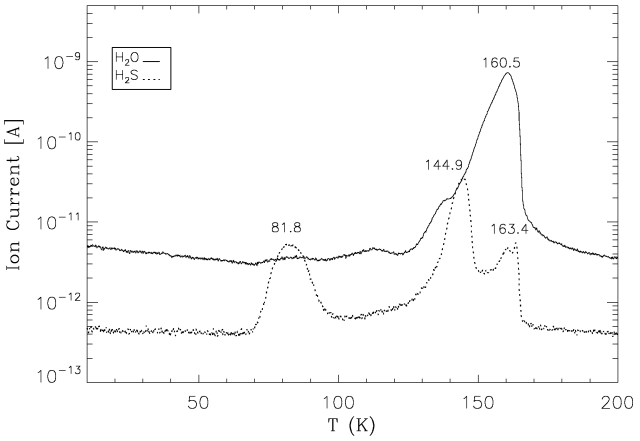

Fig. 4. Thermal desorption of the H_2S:H_2O = 7.5:100 ice mixture, with a heating rate of 1 K min^{-1}, corresponding to experiment S6 of Table 1. The ion current in Ampere, represented on the y-scale, corresponds roughly to the partial pressure in mbar.

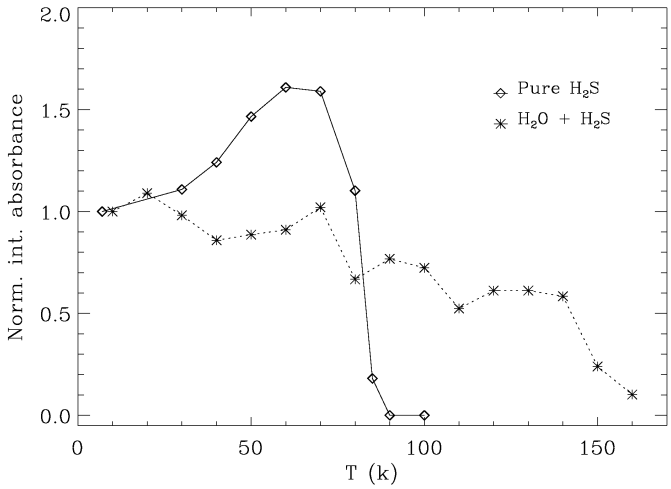

Fig. 5. Normalized integrated infrared absorbance of pure H_2S ice (experiment S3) and H_2S:H_2O = 7.5:100 ice (experiment S6, see Table 1) at different temperatures during warm-up.

The effect of the H_2O-matrix on the desorption of H_2S ice was also monitored by integrating the infrared H_2S absorption band for pure H_2S and for the H_2S:H_2O = 7.5:100 ice mixture at different temperatures during warm-up, see Figs. 1 and 3. The values of the integrated absorbance are shown in Fig. 5. It is important to note that the QMS data presented in Figs. 2 and 4 reflects the detection of desorbed molecules in the gas phase, while the integrated infrared absorbances not only show a decrease in the infrared band due to desorption, they are also affected by crystallization. First, the main difference between the pure H_2S ice and the H_2S:H_2O = 7.5:100 ice experiments is the crystallization process, as seen in Fig. 5: while no increase in the integrated absorbance is observed in the H_2S:H_2O = 7.5:100 ice experiment, the high rise of the integrated absorbance for pure H_2S ice is due to crystallization. The band strength of $A(H_2S) = 2.9 \times 10^{-17}$ cm molecule^{-1} commonly used (Smith 1991) refers to H_2S at 80 K when full crystallization is attained. We obtained a band strength value at 10 K of $A(H_2S) = 2.0 \times 10^{-17}$ cm molecule^{-1}, using the expression

$$A_{10\,\mathrm{K}} = \frac{\mathrm{Int.abs}_{10\,\mathrm{K}}}{\mathrm{Int.abs}_{70\,\mathrm{K}}} A_{70\,\mathrm{K}} \quad (4)$$

where $A_{10\,\mathrm{K}}$ and $A_{70\,\mathrm{K}}$ are the band strength values of H_2S at 10 and 70 K, respectively, $\mathrm{Int.abs}_{10\,\mathrm{K}}$ and $\mathrm{Int.abs}_{70\,\mathrm{K}}$ are the integrated absorption values of the H_2S band at 10 and 70 K. Second, the integrated absorbance of pure H_2S ice dropped to zero above 90 K; i.e., all the H_2S ice molecules have desorbed at that temperature, but in the H_2S:H_2O = 7.5:100 (experiment S6 of Table 1) ice experiment H_2S molecules are kept in the H_2O matrix up to 130 K. The much higher sensitivity of QMS compared to FTIR spectroscopy explains why desorption of H_2S is observed at temperatures above 130 K by QMS during the same experiment, see Fig. 4 and its interpretation as given above.

3.2. Irradiation of pure H_2S ice experiments

Upon photolysis of H_2S, the formation of $HS^{\cdot}$ radicals occurs, following the reaction

$$H_2S + h\nu \xrightarrow{k_1} HS^{\cdot} + H^{\cdot}. \quad (5)$$

Two radical-radical reactions are then possible:

$$HS^{\cdot} + H^{\cdot} \xrightarrow{k_2} H_2S, \quad (6)$$

reforming the H_2S molecule or

$$HS^{\cdot} + HS^{\cdot} \xrightarrow{k_3} H_2S_2. \quad (7)$$

Further irradiation leads to the photolysis of the reformed H_2S. According to Isoniemi et al. (1999) which used a 266 nm ND:YAG laser as UV source to irradiate H_2S_2 in solid Ar, the following reactions can occur:

$$H_2S_2 + h\nu \xrightarrow{k_4} HS_2^{\cdot} + H^{\cdot}, \quad (8)$$

$$H_2S_2 + h\nu \xrightarrow{k_5} S_2 + H_2, \quad (9)$$

$$HS_2^{\cdot} + h\nu \xrightarrow{k_6} S_2 + H^{\cdot}. \quad (10)$$

The top panel of Fig. 6 shows the infrared spectra of H_2S ice at 7 K for different irradiation times, corresponding to experiment S8 of Table 1. After irradiation, the sample was warmed-up at a rate of 1.4 K min^{-1}. The infrared spectra of the irradiated sample, collected at different temperatures during warm-up, are shown in the bottom panel of Fig. 6. Similar to the infrared spectra of the experiment with no irradiation, S2 shown in Fig. 1, the spectral changes observed on the irradiated sample during warm-up, see bottom panel of Fig. 6, are due to crystallization of the H_2S ice fraction that remains after the photolysis. According to Isoniemi et al. (1999), the reaction rate constants corresponding to reactions 8, 9, and 10 are, respectively, $k_4 = 0.041$ min^{-1} $k_5 = 0.035$ min^{-1}, and $k_6 = 0.006$ min^{-1} for irradiation with a 266 nm laser. For short irradiation times reaction 9 dominates the production of S_2, but after a certain time reaction 10 becomes more important.

The intricate network of reactions described above yields several products, with overlapping infrared absorption bands. It was therefore not possible to distinguish between the different irradiation products. The absorption band centered near 2550 cm^{-1}, see Fig. 6, is attributed to the S−H stretching modes of H_2S, H_2S_2, and $HS^{\cdot}$, as well as their dimers. We attribute the main contribution of the neighboring band at 2483 cm^{-1} to the S−H stretching modes of the $HS_2^{\cdot}$ radical. Based on Isoniemi et al. (1999), other authors assign the same 2483 cm^{-1} band to the S−H stretching modes of H_2S_2 (Moore et al. 2007). Isoniemi et al. (1999) give the values of 2463 and 2460 cm^{-1}

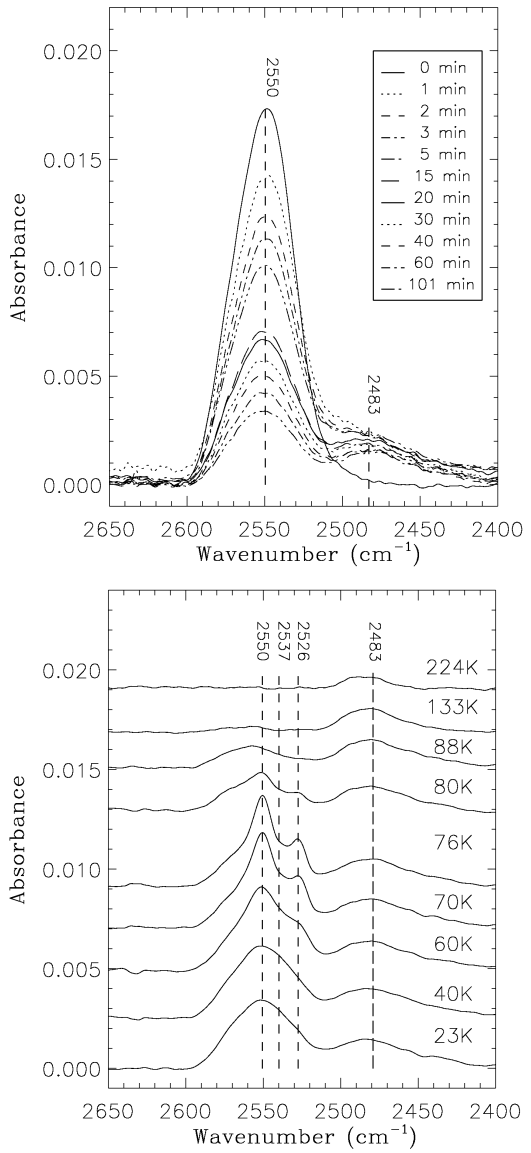

Fig. 6. *Top*: infrared spectra of H_2S ice at 7 K for different irradiation times, corresponding to experiment S8 of Table 1. *Bottom*: for the same experiment, infrared spectra of the irradiated sample collected at different temperatures during warm-up.

for the $HS_2^{\cdot}$ radical, while the values assigned to H_2S_2 are 2554 and 2557 cm^{-1} in Ar matrix. The band position of different complexes of H_2S_2 are above 2499 cm^{-1} and therefore the 2483 cm^{-1} band is not due to H_2S_2. Comparing our data with that of Isoniemi et al. (1999), the S−H stretching modes of H_2S_2 are contained in the 2550 cm^{-1} band. Therefore, we consider that the most plausible carrier of the 2483 cm^{-1} band is the $HS_2^{\cdot}$ radical, rather than H_2S_2. These overlaps mean we could not determine the formation and destruction rate constants of all the processes involved in the irradiation of H_2S. We will see that our experimental data only allowed the calculation of reaction rate values $k_4 + k_5$, and k_6. In particular, the reformation of H_2S according to reaction 6 could not be monitored by FTIR spectroscopy. We therefore discuss a simplified kinetics scheme that assumes that photolysis of H_2S, yielding $HS^{\cdot}$, and subsequent formation of H_2S_2 as a first product, are fast processes that cannot be monitored using our FTIR spectrometer. For that reason, instead of $[H_2S]_0 = 1$ we consider that the H_2S has already been converted to H_2S_2 after a short irradiation time and use the initial conditions $[H_2S_2]_0 = 1$, $[HS_2^{\cdot}]_0 = [S_2]_0 = 0$. We then check that such approximation provides a fair fit of the experimental data. Following Isoniemi et al. (1999) we have the concentrations

$$[H_2S_2] = \exp[-(k_4 + k_5)t], \quad (11)$$

$$[HS_2] = C\{\exp[-(k_4 + k_5)t] - \exp[-k_6 t]\}, \quad (12)$$

$$[S_2] = 1 - [H_2S_2] - [HS_2]. \quad (13)$$

The condition $[S_2]_0 = 0$ implies that $\frac{d[S_2]}{dt}|_0 = 0$. Substitution of Eqs. (11) and (12) in Eq. (13), taking the first time derivative on both sides leads to $C = \frac{k_4+k_5}{k_6-k_4-k_5}$ in Eq. (12). The numerator of C, $k_4 + k_5$, differs from that given by Isoniemi et al. (1999), k_4. But our expression of C is obtained analytically as explained above and should be correct. Equation (11) was used to fit the data presented in the top panel of Fig. 7, and Eq. (12) to fit the bottom panel of Fig. 7. These fits lead to $k_4+k_5 = 0.19$, 0.11, and 0.28 min^{-1} and $k_6 = 0.07$, 0.08, and 0.06 min^{-1} for experiments S7, S8, and S9, respectively. The data points in the top panel of Fig. 7 are reasonably well fitted if we consider that the initial destruction of H_2S leading to H_2S_2 formation is not taken into account in our simplified kinetics scheme. In addition, refractory residue formation was also not considered.

The top panel of Fig. 7 also displays how the rate constants are linked to the ice thickness, showing that the largest destruction (of 96%) corresponds to the thinnest ice, S9, while the lowest destruction (of 82%) corresponds to the thickest ice, S8, see Table 1. The same process (k_4+k_5) can also be monitored by following the formation of $HS_2^{\cdot}$ during UV irradiation of H_2S. This is shown in the bottom panel of Fig. 7 where the abundances of $HS_2^{\cdot}$ with respect to H_2S, associated to the 2483 cm^{-1} band are displayed.

However, additional elongation reactions of $HS_2^{\cdot}$ are probably present and compete with S_2 formation, elongating the $HS_2^{\cdot}$ molecule up to H_2S_8 and finally forming S_8. The polymerization process is favored by the high $N_s(HS_2^{\cdot})/N_s(H_2S)$ ratio in the first minutes of irradiation encouraging the reaction between two $HS_2^{\cdot}$ molecules. This could explain the higher abundance of $HS_2^{\cdot}$ in the first stages of irradiation with respect to the final irradiation time for the thinnest ice, which has the lowest rate ($k_6 = 0.06$ min^{-1}).

H_2SS might also be a product of H_2S ice photoprocessing in our experiments. It has a greater energetic level than its H_2S_2 isomer, roughly 160 kJ mol^{-1} larger (Gerbaux et al. 2000). Nevertheless, H_2SS has a lower stability, due to its energetic sizable barrier that prevents rearrangement back to the more stable H_2S_2 form at cryogenic temperatures. Thermal isomerization of H_2S_2 leading to H_2SS can therefore be excluded, and H_2SS should be kinetically stable toward unimolecular isomerization at low temperatures (Steudel et al. 1997). For this reason, only a photochemical process can explain the formation of H_2SS. Two different reactions can generate H_2SS:

$$H_2S + S^{\cdot} \xrightarrow{k_7} H_2SS, \quad (14)$$

and

$$HS_2^{\cdot} + H^{\cdot} \xrightarrow{k_8} H_2SS. \quad (15)$$

The infrared frequencies of H_2SS have been calculated by different methods, where the ν_2(HSH-bending) of H_2SS is expected to fall at 1236 cm^{-1} (Isoniemi et al. 1999). During UV irradiation of H_2S ice, a new band grows well above the noise level at 1233 cm^{-1} with a signal-to-noise ratio of 3.7. This band is

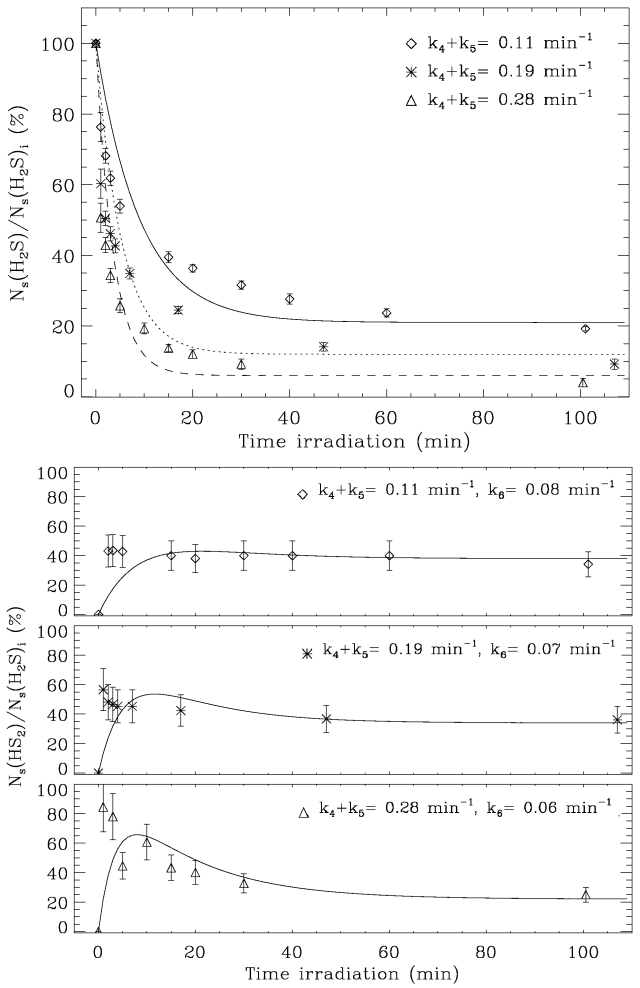

Fig. 7. Destruction of H_2S and formation of $HS_2^{\cdot}$ during UV irradiation. *Top*: data points corresponding to S7 (asterisks), S8 (diamonds), and S9 (triangles) experiments, see Table 1. For each experiment, the integrated absorbance values of the 2550 cm^{-1} band of H_2S ice as a function of UV irradiation time, $N_s(H_2S)$, were normalized with respect to their initial values before irradiation, $N_s(H_2S)_i$. The fits were made using Eq. (11) and rate constant values displayed in the figure. Error bars represent the standard deviation in each experiment. *Bottom*: normalized integrated absorbance values of the 2483 cm^{-1} band attributed to the $HS_2^{\cdot}$ product as a function of UV irradiation time, corresponding to S7 (asterisks), S8 (diamonds), and S9 (triangles), see Table 1. Normalization was done with respect to the integrated absorbance values of the 2483 cm^{-1} band after the same irradiation time. The solid line is a fit using Eq. (12) and rate constants displayed in the figure.

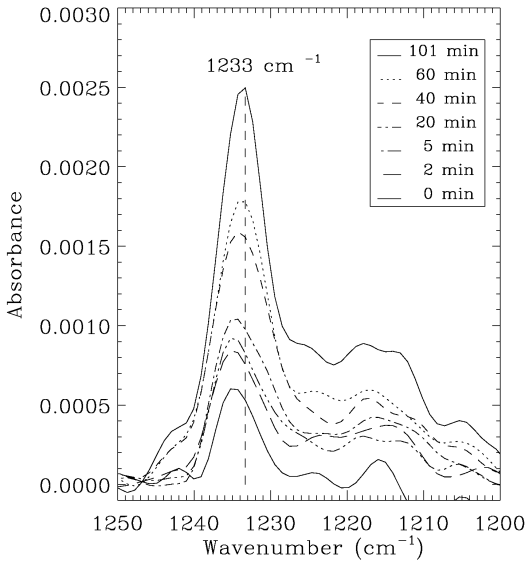

Fig. 8. Infrared band around 1233 cm^{-1} formed by UV irradiation of H_2S ice at 7 K, corresponding to experiment S8 of Table 1. Spectra were collected for different irradiation times, see inlet. This band is attributed to H_2SS based on calculations by Isoniemi et al. (1999).

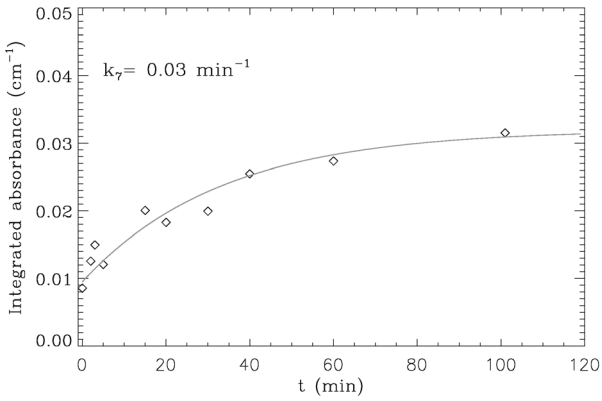

Fig. 9. Integrated absorbance values of the 1233 cm^{-1} band attributed to H_2SS ice as a function of UV irradiation time, corresponding to experiment S8, see Table 1. The solid line is a first-order fit using rate constant k = 0.03 min^{-1}, which is probably the value of k_7 from Eq. (14).

shown for different irradiation times in Fig. 8, and the corresponding integrated absorbance values are shown in Fig. 9. The solid line is the fit, giving k_7 = 0.03 min^{-1}. The position and the growth of this band as a function of irradiation time suggests that its molecular carrier is H_2SS.

UV irradiation of H_2S ice leads to the formation of S-polymers, which were detected at room temperature by chromatographic techniques (Muñoz Caro 2002), see Sect. 1. Figure 10 shows the TPD spectra corresponding to the H_2S_2, S_2, and S_3 products, measured during the warm-up of experiment S8, see Table 1. The peaks at 178 and 138 K in the m/z = 66 spectrum may be due to the cis- and trans- isomers of H_2S_2, which could be formed by reclustering of $HS_2^{\cdot}$ during warm-up. The desorption temperature of the cis-isomer is higher because its packing energy is greater than that of the trans-isomer, although the former has less stability than the latter (Cárdenas-Jirón et al. 1990). The lower stability of the cis-isomer is a more prominent steric effect, because their hydrogens are partially eclipsed. Alternatively, the same peaks at 178 and 138 K could be attributed to a mixture of H_2S_2 and H_2SS.

The peaks at 212 and 275 K most likely correspond to S_2, and S_3, respectively. The formation of S_2 and S_3 in the ice cannot be observed by mid-infrared spectroscopy. Addition of $S^{\cdot}$ or $SH^{\cdot}$ to other species such as H_2S_2, $HS_2^{\cdot}$, and $S_2^{\cdot}$ lead to formation of S_3 and other S-polymers up to S_8 (Barnes et al. 1974).

3.3. Irradiation of H_2O:H_2S ice experiments

The H_2S:H_2O = 4.0:100 ice mixture was irradiated at 8 K, see experiment S10 of Table 1 for experimental parameters. The corresponding infrared spectra for different irradiation times are displayed in Fig. 11. While the H_2S band at 2546 cm^{-1} decreases as a function of irradiation time, two new bands appear at 1328

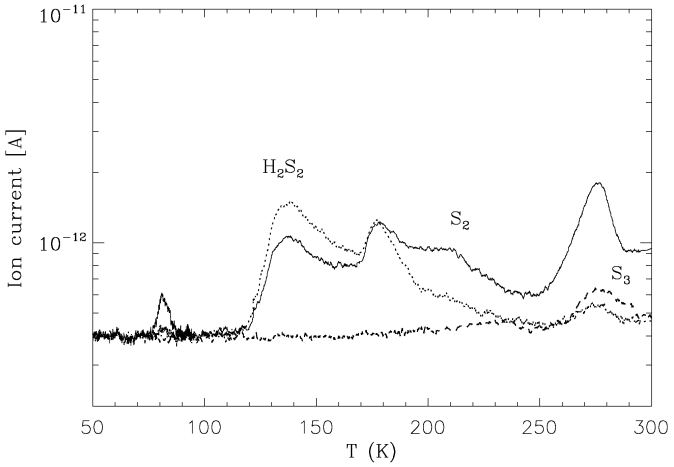

Fig. 10. Thermal desorption of UV-irradiated H_2S ice, corresponding to experiment S8 of Table 1. Spectra correspond to m/z = 66 (dotted trace), m/z = 64 (solid trace), m/z = 96 (dashed trace), the molecular ion masses of the H_2S_2, S_2, and S_3 products. The ion current in Ampere, represented on the y-scale, corresponds roughly to the partial pressure in mbar.

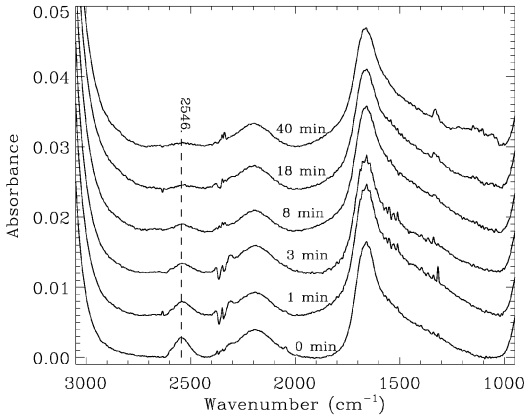

Fig. 11. Infrared spectra of the H_2S:H_2O = 4.0:100 ice mixture at 8 K for different irradiation times, corresponding to experiment S10 of Table 1.

and 1151 cm^{-1}, and the latter is very weak, which correspond to the asym. and sym. str. modes of SO_2.

Other weak bands appeared in the 1300−1000 cm^{-1} region. To characterize these bands better we performed a simultaneous deposition and irradiation experiment with the less diluted H_2S:H_2O = 13:100 ice mixture, experiment S12 of Table 1. The infrared spectra of the irradiated sample, collected at different temperatures during warm-up, are shown in Fig. 12. The SO_2 bands are also observed in this experiment. Two new bands near 1110 and 1052 cm^{-1} are associated to $SO_4^=$ and HSO_4^-, based on previous assignments by Kunimatsu et al. (1988) and Moore et al. (2007). These species correspond to higher oxidation states of photoprocessed SO_2.

Upon warm-up the band of HSO_4^- at 1052 cm^{-1} decreases and the $SO_4^=$ band at 1110 cm^{-1} shifts to 1083 cm^{-1} at 180 K, when its intensity is maximum. After water desorption, H_2SO_4 tetrahydrate formed at 180 K. At 190 K new absorption bands appear at 1142, 1024, and 901 cm^{-1}. These absorption bands indicate the presence of H_2SO_4 monohydrate. At 220 K the bands observed at 1374 and 954 cm^{-1} can be interpreted as a mixture of H_2SO_4 in its pure state and H_2SO_4 monohydrate, following the

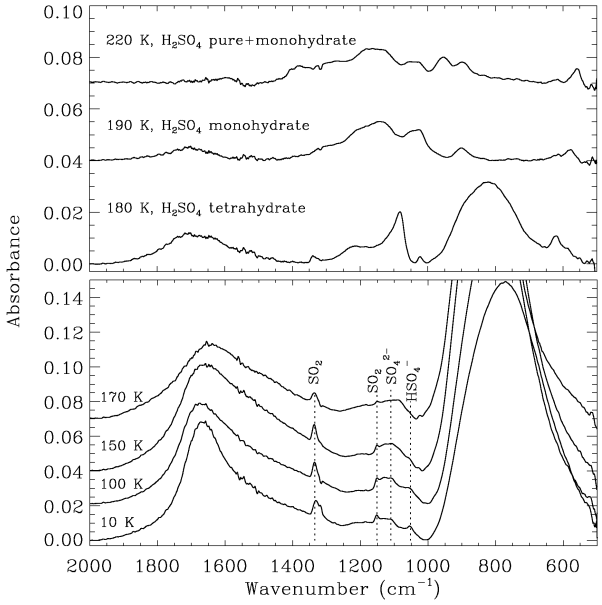

Fig. 12. Infrared spectra of the H_2S:H_2O = 13:100 ice mixture for different temperatures deposited at 8 K, corresponding to experiment S12 of Table 1. The deposition and irradiation was performed simultaneously in this experiment.

Moore et al. (2007) assignment. This ejection of water continues up to room temperature (Couling et al. 2002).

TPD curves of H_2S:H_2O = 13:100 ice in the 90−143 K range are shown in Fig. 13. A desorption peak present at 106 K is common to the m/z = 16, 32, 48, 64, and 66 spectra. These mass fragments correspond to H_2SO_2 or a mixture of H_2SO_2 and SO_2. The H_2SO_2 molecule has not been previously detected, but it is thought to be necessary as an oxidation intermediate to yield oxides with elevated oxidation states (Steiger & Steudel 1992). Desorption of SO_2 at 128 K is observed as an increase in the m/z = 16, 48, 64 spectra. Overlapping with the desorption of SO_2 is another peak around 137 K common to m/z = 32, 64, 66. This desorption is assigned to H_2S_2, which desorbed at a similar temperature, 138 K, in the pure H_2S irradiation experiment, see Fig. 10. Two of the above products, H_2S_2 and SO_2, were detected by infrared spectroscopy after proton bombardment of the H_2O:H_2S = 8:1 ice mixture; the other products detected by us in the H_2S:H_2O UV irradiation experiments, were formed by proton bombardment of H_2O:SO_2 ice mixtures (Moore et al. 2007).

The TPD curves of the same H_2S:H_2O = 13:100 ice irradiation experiment in the 140−205 K range are displayed in Fig. 14. A desorption peaking at 149 K is common to m/z = 16, 32, 64, 66, and 81. This combination of mass fragments corresponds to a possible desorption of the HSO_3^- anion. No desorption of mass fragment m/z = 82, corresponding to H_2SO_3, was observed.

Both infrared and QMS data, Figs. 12 and 14, show that a large fraction of the irradiation products mentioned above is retained in the H_2O-matrix and finally co-desorb with H_2O between 160−190 K. Also a fraction of the more refractory H_2SO_4, m/z = 98, co-desorbs with H_2O around 175 K, see Fig. 14.

4. Astrophysical implications

Comparison of our laboratory spectra with observations of YSOs, performed with the ISO satellite, show an absorption band compatible with the 2548 cm^{-1} (3.925 μm) feature of solid

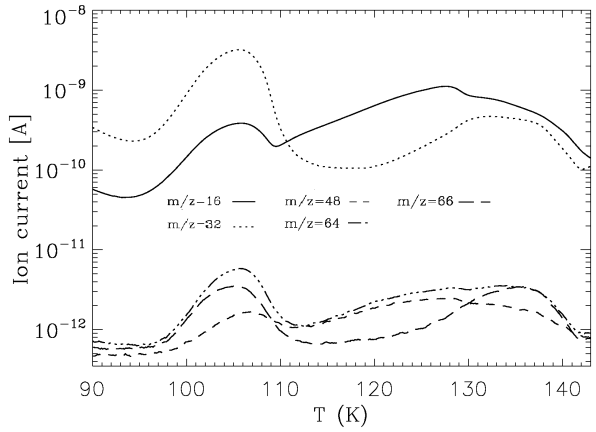

Fig. 13. Thermal desorption of UV-irradiated H_2S:H_2O = 13:100 in the range of 90–140 K, corresponding to experiment S12 of Table 1. The ion current in Ampere, represented on the y-scale, corresponds roughly to the partial pressure in mbar.

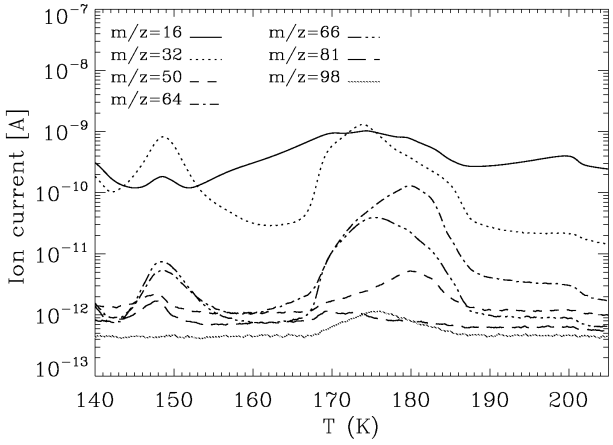

Fig. 14. Thermal desorption of UV-irradiated H_2S:H_2O = 13:100 in the 140–205 K range, corresponding to experiment S12 of Table 1. The ion current in Ampere, represented on the y-scale, corresponds roughly to the partial pressure in mbar.

H_2S in the ice mantles. The absorbances toward different YSOs were calculated as follows

$$Absorbance = -\log_{10}\left(\frac{I}{I_0}\right) \quad (16)$$

where I is the flux, in Jy, measured toward the YSO line of sight, and I_0 is the continuum flux.

Methanol ice displays two weak bands at 2530 and 2610 cm^{-1} (3.95 and 3.83 μm), which are assigned to the combination modes (Dartois et al. 1999), and can overlap with the H_2S absorption at 2548 cm^{-1} (3.925 μm). The fit of the 3.95 μm feature with the laboratory spectrum of pure CH_3OH allows setting an upper limit on the 3.83 μm CH_3OH absorption. In addition, the ~18 cm^{-1} (0.025 μm) difference in the position of the H_2S feature at 3.925 μm with respect to the CH_3OH feature at 3.95 μm also allows differentiation of both absorptions. It is therefore possible to provide an upper limit on the value of $N(H_2S)$.

The column density of CH_3OH toward W33A, $N(CH_3OH)$, which is obtained from integration of the 3.95 and 3.83 μm bands, is about 2×10^{18} cm^{-2} (Dartois et al. 1999) from UKIRT observations. The different values of $N(CH_3OH)$ depend on

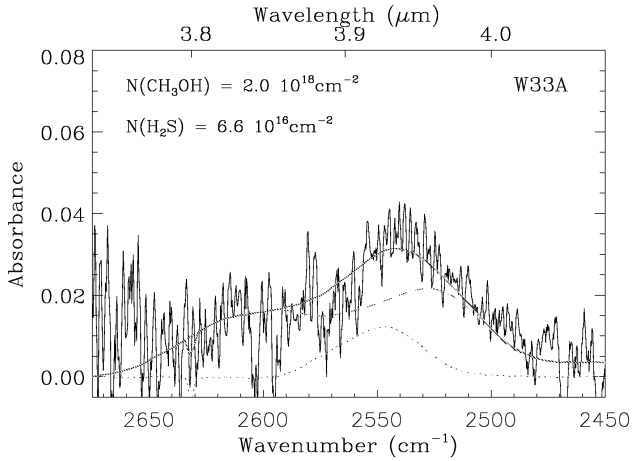

Fig. 15. Comparison between our experimental data and the ISO observation of W33A. Dashed line corresponds to the pure CH_3OH ice spectrum at 20 K, dotted line corresponds to pure H_2S ice at 20 K, and the continuous line is the addition of both spectra.

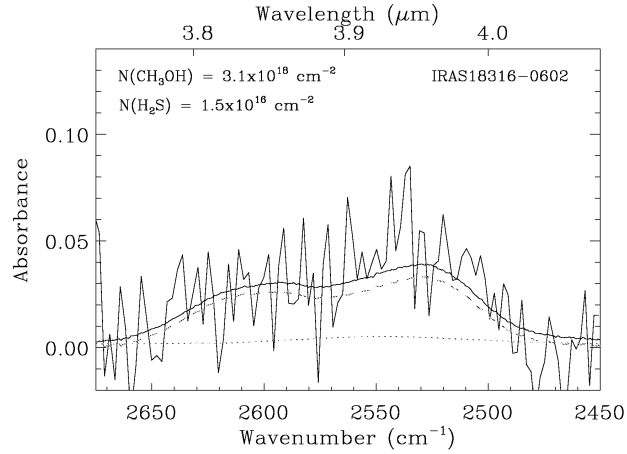

Fig. 16. Comparison between our experimental data and the ISO observation of IRAS18316-0602. Dashed line corresponds to the pure CH_3OH ice spectrum at 20 K, dotted line corresponds to the H_2S:H_2O = 13.7:100 ice mixture at 20 K, and continuous line is the addition of both spectra.

the infrared band used for integrating the absorbance and the telescope used. For instance, Allamandola et al. (1992) obtain $N(CH_3OH) = 4.0 \times 10^{18}$ cm^{-2} from integration of the 2825 cm^{-1} (3.53 μm) band toward W33A using the 3 m telescope at IRTF. Figure 15 shows the spectrum of protostar W33A, which is similar to what is reported by Teixeira et al. (1999) from ISO observations. The laboratory fit consists of adding pure CH_3OH and pure H_2S ice spectra, both at 20 K. We obtained $N(CH_3OH) = 2.0 \times 10^{18}$ cm^{-2} and $N(H_2S) \leq 6.6 \times 10^{16}$ cm^{-2}, as shown in Table 2.

The best fit of protostar IRAS18316-0602 spectrum, shown in Fig. 16, is obtained by adding the spectrum of pure CH_3OH at 20 K with that of the H_2S:H_2O = 13.7:100 ice mixture at 20 K. The column density of pure CH_3OH toward this source is $N(CH_3OH) = 3.8 \times 10^{18}$ cm^{-2} (Dartois et al. 1999) using the UKIRT telescope. We obtained column density values of $N(CH_3OH) = 3.1 \times 10^{18}$ cm^{-2} and $N(H_2S) \leq 1.5 \times 10^{16}$ cm^{-2} from ISO observations, see Table 2.

The upper limits of 0.7% and 0.13% for the H_2S abundances given in Table 2, corresponding to W33A and IRAS18316-0602, are well below the H_2S/H_2O = 1/37 abundance ratio

Table 2. Observed ratios toward protostars.

Source	$N(CH_3OH)$ (cm^{-2})	$N(H_2S)$ (cm^{-2})	$N(H_2O)$ (cm^{-2})	$\frac{N(H_2S)}{N(H_2O)}$ (%)
W33A	2.0×10^{18a} 2×10^{18b}	$\leq 6.6 \times 10^{16a}$	$0.9–4.2 \times 10^{19b}$	$\leq 0.7–0.2^a$
IRAS18316-0602	3.1×10^{18a} 3.8×10^{18b}	$\leq 1.5 \times 10^{16a}$	1.2×10^{19b}	$\leq 0.13^a$

Notes. [(a)] This work. [(b)] Dartois et al. (1999).

(corresponding to 2.7% H_2S relative to H_2O) based on the S/O = 1/37 cosmic abundance ratio, see Sect. 1. The products formed by UV irradiation of H_2S in ice mantles might also account for the missing sulfur in dense clouds and circumstellar regions. The more refractory products could stick to the grain even after sublimation of the ice mantle. If we assume a flux value of 10^4 photons $cm^{-2}\,s^{-1}$ in a dense cloud interior (Shen et al. 2004 and ref. therein), ice mantles experience a fluence of 3.2×10^{17} photons cm^{-2} after 10^6 yr, which using Eq. (3) with $\sigma \approx \sigma(H_2O) = 4.0 \times 10^{-18}$ cm^2 corresponds to 12% absorption or 3.8×10^{16} photons absorbed cm^{-2}. If we divide the number of absorbed photons cm^{-2} by the ice column density of 3.12×10^{16} molecules cm^{-2}, i.e. a 0.01 μm thick ice mantle we find that roughly, each molecule absorbed 1.2 photons on average. Ideally, a relevant laboratory simulation of such a process should use the same ice thickness of 0.01 μm, but a quantitative estimation of the irradiation products in this ice is not possible in practice. As a rough approximation, we made an experiment where the average number of photons absorbed per molecule is similar. Experiment S10 is the closest to those conditions. It involved the irradiation of H_2S:H_2O = 4.0:100 ice, so it was exposed to ≈0.8 photon $molecule^{-1}$. About 75% of the H_2S molecules in the ice were photoprocessed, leading to the formation of products in the experiment. Among the H_2S-photoprocessing products that could be present in ice mantles, H_2S_2 and $HS^{\cdot}$ are difficult to detect because their absorptions overlap with the H_2S band near 2548 cm^{-1} (3.925 μm). The neighboring band at 2483 cm^{-1} (4.027 μm), attributed to the $HS_2^{\cdot}$ and H_2SS species, see Sect. 3.2 and top panel of Fig. 6, is expected to be below the detection limit of current infrared observations. With the exception of the SO_2 detection (Boogert et al. 1997) in circumstellar ice mantles, the oxidized S species, formed by irradiation of H_2S:H_2O ice mixtures, Sect. 3.3, have so far not been detected by infrared spectroscopy, although SO_2 species has been detected in the solid phase. Other products of H_2S-photoprocessing are the S-polymers, from S_2 to S_8, and organic species containing S (Muñoz Caro 2002). Atomic S was detected by ISO at 25.2 μm in the Orion H_2 emission peak (Rosenthal et al. 2000). Rotational transitions of sulfur chains will be observable with ALMA (Wakelam et al. 2005). Cyclic S_8 is active in the infrared region, but has not been observed in the emission spectra of comets. It could be detected by simple in situ GC-MS analysis, i.e. without derivatization, of a comet nucleus planned by the ongoing Rosetta mission (Muñoz Caro 2002; Goesmann et al. 2007).

5. Conclusions

We determined the desorption temperature of H_2S ice, which depends on the initial H_2S/H_2O ratio. Pure H_2S ice desorbs around 82 K. When H_2S is present in an H_2O ice matrix, a fraction of the H_2S co-desorbs with H_2O in the 130–170 K temperature range, showing two maxima around 145 and 163 K. These results agree with Collings et al. (2004). Comparison of the laboratory infrared spectra of H_2S, pure or in an H_2O matrix, with ISO observations of protostars W33A and IRAS18316-0602 provided upper limits of 0.7 and 0.13% on the solid H_2S abundance relative to H_2O. These values are too low to explain the S depletion observed toward dense clouds and circumstellar regions. Another reservoir of S in these regions could be the products of H_2S ice photoprocessing. It was found that solid H_2S, which expected in icy grain mantles, photolyzes very readily, leading to the formation of several species, including H_2S_2, $HS^{\cdot}$, $HS_2^{\cdot}$, S_2, and H_2SS. The set of reactions leading to these species is known, and it was possible to determine the values of some of the rate constants involved. If H_2S was present in an H_2O ice matrix the SO_2, $SO_4^{=}$, HSO_3^{-}, HSO_4^{-}, H_2SO_2, H_2SO_4, and H_2S_2 photoprocessing products were formed in our experiments. Proton bombardment of H_2S:H_2O ice led to formation of H_2S_2 and SO_2, while a similar processing of SO_2:H_2O ice formed H_2O_2, H_3O^+, HSO_3^{-}, HSO_4^{-}, and $SO_4^{=}$ (Moore et al. 2007). With the exception of H_2SO_4, all the above products of H_2S:H_2O ice photoprocessing desorbed between 100–200 K. S-polymers from S_3 to S_8 are also products of H_2S photoprocessing; these species can stick on grains even after sublimation of the ice mantle (Muñoz Caro 2002, this work). In general, given the expected relative low abundances of S-polymers in ice mantles, they would be difficult to detect by infrared spectroscopy, but some of them will be observable with ALMA in the gas phase (Wakelam et al. 2005). The UV-irradiation of H_2O:CO:CH_3OH:NH_3:H_2S ices is left for future work. It was found that S_8 was by far the most abundant refractory product in these experiments, even for low initial H_2S ice abundances on the order of 2% relative to H_2O ice (Muñoz Caro 2002). Including C in H_2S-containing ices, in the form of abundant ice components such as CH_3OH or CO, may lead to species like OCS, which is observed in circumstellar ice mantles.

Acknowledgements. We acknowledge U. J. Meierhenrich and W. A. Schuttte for collaboration on previous experiments involving chromatographic analysis of residues made from UV-irradiation of H_2S-containing ice, published in the Ph.D. thesis of G. M. M. C. We thank J. R. Goicoechea for his support in reducing ISO data and J. Sobrado for technical support. We also thank the ISO database and W. Frieswijk et al. for providing the data collection and previous data processing of spectra of W33A and IRAS18316-0602. A.J. was financed by a training grant from INTA. G.M.M.C. was supported by a Ramón y Cajal research contract from the MICINN in Spain. This research was financed by the Spanish MICINN under Project AYA2008-06374 and CONSOLIDER grant CSD2009-00038.

References

Allamandola, L. J., Sandford, S. A., & Tielens A. G. G. M. 1992, ApJ, 399, 134.
A'Hearn, M. F., Schleicher, D. G., & Feldman, P. D. 1983, ApJ, 274, L99

A'Hearn, M. F.,Arpigny, C., Feldman, P. D., et al. 2000, Am. Astr. Soc., 32, 1079
Barnes, A. J., Hallam, H. E., & Howels, J. D. R. 1974, J. Mol. Struct., 23, 463
Bockelée-Morvan, D., Lis, D. C., Wink, J. E., et al. 2000, A&A, 353, 1101
Boogert, A. C. A., Schutte, W. A., Tielens, A. G. G. M., et al. 1997, A&A, 315, L377
Buckle, J. V., & Fuller, G. A. 2003, A&A, 399, 567
Cárdenas-Jirón, G. I., Cárdenas-Lailhacar, C., & Toro-Labbe, A. 1990, J. Mol. Struct., 210, 279
Couling, S. B., Sully, K. J., & Horn, A. B. 2002, J. Am. Chem. Soc., 125,
Collings, M. P., Anderson, M. A., Chen, R., et al. 2004, MNRAS, 354, 1133
Dartois, E., Geballe, T. R., Demyk, K., Ehrenfreund, P., & d'Hendecourt, L. 1999, A&A, 342, L32
Doty, S. D., Schoier, F. L., & van Dishoeck, E. F. 2004, A&A, 418, 1021
Ferrante, R. F., Moore, M. H., Spiliotis, M. M., & Hudson, R. L. 2008, ApJ, 684, 1210
Garozzo, M., Fulvio, D., Kanuchova, Z., Palumbo, M. E., & Strazzulla, G. 2010, A&A, 509, A67
Geballe, T. R. 1991, MNRAS, 251, 24
Geballe, T. R., Baas, F., Greenberg, J. M., & Schutte, W. 1985, A&A, 146, L6
Gerbaux, P., Salpin, J.-Y., Bouchoux, G., & Flammang, R. 2000, Int. J. Mass Spectrometry, 195/196, 239
Goesmann, F., Rosenbauer, H., Roll, R., et al. 2007, Space Sci. Rev., 128, 257
Grim, R. J. A., & Greenberg, J. M. 1987, A&A, 181, 168
Hagen, W., Tielens, A. G. G. M., & Greenberg, J. M. 1981, Chem. Phys., 56, 367
Hudgins, D. M., Sandford, S. A., Allamandola, L. J., & Tielens, A. G. G. M. 1993, AJSS, 86, 713
Irvine, W. M., Schloerb, F. P., Crovisier, J., Fegley, B., Jr., & Mumma, M. J. 2000, in Protostars and Planets IV, ed. V. Mannings, A. P. Boss, & S. S. Russell (Univ. Arizona Press: Tucson), 1159
Isoniemi, E., Khriachtchev, L., Pettersson, M., & Rasanen, M. 1999, Chem. Phys. Lett., 311, 47
Kunimatsu. K., Samant, M. G., & Philpott, M. R. 1988, J. Electroanal. Chem., 243, 203
Laffont, C., Boice, D. C., Andernach, H., et al. 1996, Am. Astr. Soc., 28, 1094
Lee, L. C., Wang, X., & Suto, M., 1987, J. Chem. Phys., 86, 8
Mason, N. J., Dawes, A., Holton, P. D., et al. 2006, Faraday Discuss., 133, 311
Moore, M. H., Hudson, R. L., & Carlson, R. W. 2007, Icarus, 189, 409
Muñoz Caro, G. M. 2002, Ph.D. Thesis
Muñoz Caro, G. M., Jiménez-Escobar, A., Martín-Gago, J. Á., et al. 2010, A&A, 522, A108
Palumbo, M. E., Tielens, A. G. G. M., & Tokunaga, A. T. 1995, ApJ, 449, 674
Rosenthal, D., Bertoldi, F., & Drapatz, S. 2000, A&A, 356, 705
Shen, C. J., Greenberg, J. M., Schutte, W. A., & van Dishoeck, E. F. 2004, A&A, 415, 203
Smith, R. G. 1991, MNRAS, 249, 172
Snow, T. P., & Witt, A. N. 1996, ApJ, 468, L65
Steiger, T., & Steudel, R. 1992, J. Molec. Struct., 257, 313
Steudel, R., Drozdova, Y., Miaskiewicz, K., Hertwig, R. H., & Koch, W. 1997, J. Am. Chem. Soc., 119, 1990
Teixeira, T. C., Devlin, J. P., Buch, V., & Emerson, J. P. 1999, A&A, 347, L19
Tieftrunk, A., Pineau des Forets, G., Schilke, P., & Walmsley, C. M. 1994, A&A, 289, 579
van der Tak, F. F. S., Boonman, A. M. S., Braakman, R., & van Dishoeck, E. F. 2003, A&A, 412, 133
Wakelam, V., Castets, A., Ceccarelli, C., et al. 2004, A&A, 413, 609
Wakelam, V., Caselli, P., Ceccarelli, C., et al. 2005, Proc. The Dusty and Molecular Universe, Paris, France 2004 (ESA SP-577)
Weber, P., & Greenberg, J. M. 1985, Nature, 316, 403